ORGANOMETALLICS

Article

pubs.acs.org/Organometallics

# Synthesis, Cyclization, and Migration Insertion Oligomerization of $CpFe(CO)_2(CH_2)_3PPh_2$ in Solution

Kai Cao, Brian Tsang, Yibo Liu, Daniel Chelladural, William P. Power,* and Xiaosong Wang*

Department of Chemistry and Waterloo Institute for Nanotechnology (WIN), University of Waterloo, 200 University Avenue, Waterloo, Canada N2L 3G1

Supporting Information

**ABSTRACT:** Cyclopentadienyldicarbonyl[(diphenylphosphino)propyl]-iron ($CpFe(CO)_2(CH_2)_3PPh_2$, FpP), containing both Fp and phosphine groups, was synthesized as a difunctional monomer for migration insertion polymerization (MIP). FpP underwent either intra- or intermolecular reactions in solution. When a solution with low FpP concentration (ca.1% by weight) was left at 25 °C, FpP was quantitatively converted to the five-membered-ring species **1** via CO release. On the other hand, when a solution at the same low concentration was heated to 70 °C in the dark, an intramolecular migration insertion reaction was promoted, leading to a high conversion of FpP (ca. 70%) to the six-membered cyclic Fp acyl derivatives **2**. At the same temperature with an increase in the concentration of FpP to 10% by weight, intermolecular MIR became predominant (ca. 90%) with a low yield of ring molecules (ca. 10%). Solution polymerization of FpP (ca. 20% by weight) was therefore performed at 70 °C, which generated both THF-soluble and -insoluble macromolecules via intermolecular migration insertion reactions. The resulting macromolecules were fully characterized by using FT-IR, solution- and solid-state $^{31}P$, and $^{13}C$ NMR. The soluble macromolecules exhibit a molecular weight of ca. 4200 with a PDI value of ca. 1.24, as characterized by GPC. A kinetic study shows that the polymerization follows a step-growth mechanism.

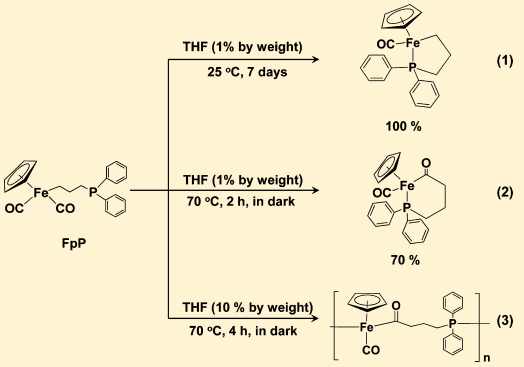


## INTRODUCTION

The convergence of organometallic and polymer chemistry has led to the emergence of an interdisciplinary research field of metal-containing polymers (MCPs).[1−5] Many MCPs exhibit interesting functions and self-assembly behavior, which render them very promising as building blocks for modern technologies.[6−16] Taking advantage of the well-developed organometallic chemistry, the synthesis of various metal-containing polymerizable compounds for processable macromolecules has therefore become a demanding but challenging research topic.[17−23] This research is essential to extend the scope of MCPs and will offer new opportunities for the future of organometallic chemistry.[24]

Migration insertion reaction (MIR)[25−27] is a well-studied organometallic reaction and has been explored for the coordination polymerization of a number of organic monomers, including olefins,[28] CO,[29] and $CO_2$,[30] for stereocontrolled organic polymers. Unlike previous reports which used metal complexes as catalysts, we have developed migration insertion polymerization (MIP), in which metal complexes acting as monomers get involved in the construction of polymer backbones. As a result, a new class of main-chain MCPs was produced.[31] The polymers are also of interest due to the presence of metal-coordinated phosphorus, which may have properties complementary to those of previously reported phosphorus-containing polymers.[32,33] It is well-known that the reaction of alkyldicarbonylcyclopentadienyliron (FpR) with nucleophilic ligands, e.g. phosphine ($PR_3$), leads to air-stable phosphine-coordinated acyl complexes as a result of MIR.[34,35] By combining both Fp and phosphine groups into one molecule via an alkyl spacer, difunctional A-B type monomers of cyclopentadienyldicarbonyl[(diphenylphosphino)propyl] iron ($CpFe(CO)_2(CH_2)_3PPh_2$, FpP) have been prepared.[31] The monomers undergo MIP, leading to air-stable poly-(cyclopentadienylcarbonyl[(diphenylphosphino)butanoyl]iron) (P-FpP) with a molecular weight of up to $10^4$.[31] The polymerization was performed in bulk in order to suppress possible intramolecular cyclic reactions. In an effort to explore solution MIP, we carried out the experiments to investigate FpP solution reaction behavior. The reactions are performed under conditions with varied FpP concentration and temperature. The results indicate that the molecules in solvents undergo both intramolecular cyclic reactions and intermolecular MIR depending on the reaction conditions (Scheme 1). At low concentration, two cyclic molecules have been produced at either low or high temperature (**1** and **2** in Scheme 1). On the other hand, at relatively higher monomer concentration, an intermolecular reaction of FpPs predominates (**3** in Scheme 1). As a result of this investigation, solution polymerization of FpP with a monomer concentration of 20% was conducted at 70 °C, resulting in both THF-soluble and insoluble PFpP.

**Received:** October 29, 2013

   dx.doi.org/10.1021/om4010516 | *Organometallics* XXXX, XXX, XXX−XXX

**Scheme 1. Solution Reactions of FpP in THF**

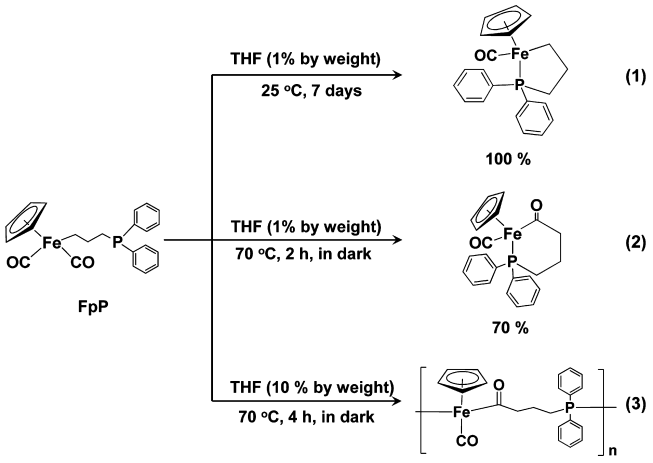


## RESULTS AND DISCUSSION

**Synthesis and Characterization of FpP.** Cyclopentadienyldicarbonyl[(diphenylphophino)propyl]iron (FpP) was synthesized via a reaction between (3-chloropropyl)diphenylphosphine and potassium cyclopentadienyldicarbonyliron.[31] The yellow oil-like form of FpP was produced most of the time, which rendered the crystallization of FpP difficult. The possible reason is attributed to the light sensitivity of Fp derivatives,[36] which may create trace amounts of impurities during the purification process. We therefore performed the reaction and purification in the dark. As a result, a yellow powder of FpP was obtained upon solvent evaporation. The yellow powder can be crystallized from hexane solution at −49 °C, resulting in single crystals suitable for X-ray diffraction. X-ray diffraction shows that the molecules crystallized in a monoclinic crystal system with space group $P2_1/c$ (Table S1, Supporting Information). As shown in Figure 1, the Fe is coordinated in a pseudo-octahedral three-legged piano-stool fashion. The Fe−C8 bond distance is 2.066 Å, and the C6−Fe−C7, C6−Fe−C8, and C7−Fe−C8 bond angles are 93.64, 85.84, and 87.29°, respectively. These structure parameters are similar to those for other Fp derivatives reported in the literature such as $[(\eta^5\text{-}C_5H_5)Fe(CO)_2]_2(CH_2)_4$ (Table S2, Supporting Information).[37] Infrared spectroscopy of the monomer shows characteristic peaks at 1952 and 2004 $cm^{-1}$ (Figure 1b), which are representative of the terminal CO groups in FpP.[25] The $^{31}P$ NMR spectrum reveals a signal at −14.7 ppm, confirming the presence of the phosphine group (Figure 1c).

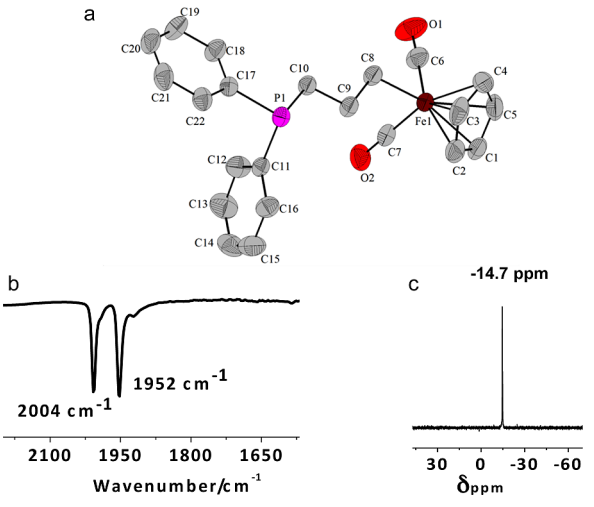


**Figure 1.** Crystal structure (a) and FT-IR (b) and $^{31}P$ NMR in DMSO-$d_6$ (c) of FpP.

The $^1H$ NMR spectrum of FpP in DMSO-$d_6$ (Figure 2a) exhibits a strong resonance at 4.8 ppm, representing the Cp ring, and a broad resonance at 7.30−7.40 ppm, representing the phenyl groups. The upfield peak at 1.46 ppm is assigned to the protons $\alpha$ and $\beta$ to Fe (a and b in Figure 2a), while the signal at 2.1 ppm is due to the protons adjacent to the phosphorus (c in Figure 2a). The integration ratio of these two peaks is 2:1 (Figure 2a), which supports the assignment. $^1H-^1H$ 2D COSY NMR of FpP in $C_6D_6$ was also performed and the spectrum is illustrated in Figure 2b. As shown in the figure, the proton signals for the propyl spacer are well separated in $C_6D_6$. The chemical shift at 1.6 ppm represents the proton $\alpha$ to Fe. The triplet at 2.2 ppm is due to the proton adjacent to phosphorus. Multiple peaks at 1.8 ppm can be assigned to the protons $\beta$ to Fe. This assignment is confirmed by the 2D chemical shift correlation map (Figure 2b). No cross peaks are observed for the signals at 1.6 and 2.2 ppm, suggesting that they are separated by the methylene in the middle of the propyl spacer.

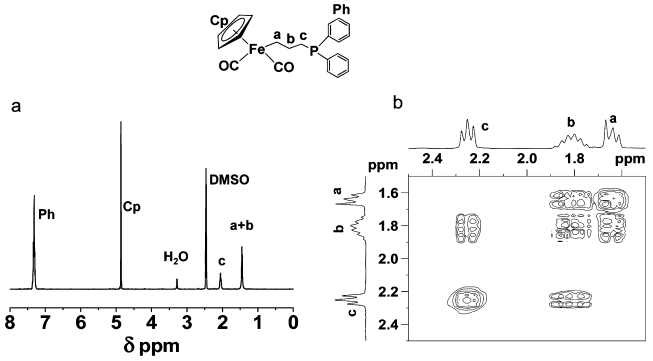


**Figure 2.** $^1H$ NMR of FpP in DMSO-$d_6$ (a) and $^1H-^1H$ COSY in $C_6D_6$ (b).

$^{13}C$ NMR of FpP in DMSO-$d_6$ shows one peak at 217 ppm representing the terminal CO group; signals due to phenyl and Cp appeared at 128−139 and 85−86 ppm, respectively (Figure S1, Supporting Information). The resonances due to the three carbons in the propyl chain (a−c in Figure S1) are observed upfield at 34.3, 32.5, and 5.1 ppm. $^{13}C-^1H$ HMQC 2D NMR of FpP in $C_6D_6$ was performed to assign these signals (Figure S1, Supporting Information). As shown in the figure, the cross peaks indicate that the signals at 5.1, 34.3, and 32.5 ppm in $^{13}C$ NMR are connected to protons a−c in the $^1H$ NMR spectrum, respectively. On the basis of this assignment, the one-, two-, and three-bond $^{13}C-^{31}P$ coupling constants for these three carbons ($^1J_{PC}$, $^2J_{PC}$, and $^3J_{PC}$) are 14, 15.3, and 11.4 Hz, respectively (inset in Figure S1). We noticed that $^2J_{PC}$ is larger than $^1J_{PC}$, which is peculiar but is commonly observed for phosphine compounds.[38]

**Cyclization Reaction of FpP.** Fp derivatives usually undergo two types of reactions in the presence of phosphine: (1) CO release followed by phosphine coordination[36] and (2) MIR at an elevated temperature.[34] FpP containing both Fp and phosphine groups is therefore expected to undergo cyclic reactions under both conditions. When an FpP solution of low


dx.doi.org/10.1021/om4010516 | Organometallics XXXX, XXX, XXX−XXX

concentration (ca. 1% by weight) in THF was exposed to light and left at room temperature for 7 days, over 99% of the FpP was converted to the five-membered-ring species **1**. On the other hand, when the solution was heated to 70 °C in the dark, the major product (ca. 70%) was the six-membered-ring species **2** via an intramolecular MIR.

To characterize **1** and **2**, single crystals suitable for X-ray crystallography were grown in hexane for **1** and in hexane/DCM (4/1) mixed solvents for **2** at −49 °C. The X-ray analysis (Figure 3) showed that both molecules crystallize in a

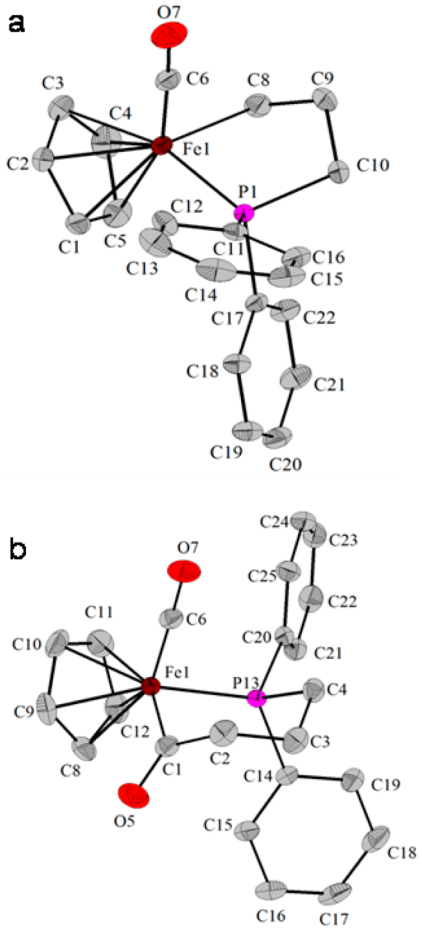


**Figure 3.** Crystal structures for **1** (a) and **2** (b).

monoclinic crystal system with space group $P2_1/c$ (Table S1, Supporting Information). Both Fe atoms in **1** and **2** assume a pseudo-octahedral coordination geometry with the Cp ring occupying three coordination sites (piano-stool configuration). The torsion angles (Tables S3 and S4, Supporting Information) indicate that all elements for the ring structures are not on the same plane. The six-membered-ring species **2** adopts a cyclohexane-like chair conformation, suggesting that low strain energy is involved in the compound.

Through comparison with previously reported data for acyclic analogues, we discovered that the formation of the cyclic structures appears to counteract the steric effect of phosphine ligands, leading to shorter P−Fe bonds. For Fp derivatives, Fe offers limited space to accommodate CO, phosphine, and one anionic ligand of $R^-$ on the three coordination sites. The size of the phosphine and R groups will therefore influence their bond distances to Fe and bond angles. For example, as shown in Table 1, for a compound with R being a bulky carborane cage ($C_2B_{10}H_{11}$),[39] the P−Fe−C angles are much larger than those

**Table 1. Comparison of Bond Angles and Distances for 1 and Its Acyclic Analogues**

| | | acyclic ($\eta^5$-$C_5H_5$)Fe(CO)($PPh_3$)R | |
|---|---|---|---|
| bond angle or distance | ring **1** | R = Et[36,40] | R = $C_2B_{10}H_{11}$[39] |
| C(8)−Fe−C(6) | 89.81(6) | 92.76(7) | 92.3(4) |
| C(6)−Fe−P | 93.60(5) | 90.61(5) | 96.4(3) |
| C(8)−Fe−P | 81.98(4) | 87.86 (5) | 99.68(1) |
| Fe−P | 2.1581(3) | 2.1699(4) | 2.271 |
| Fe−CO | 1.729(4) | 1.7291(17) | 1.729(8) |
| Fe−C(R) | 2.057(1) | 1.9601(16) | 2.093(6) |

for a compound with R being Et (Table 1). Also as a result of the steric effect, the Fe−P bond distance (2.271 Å) is much longer in comparison to 2.1699(4) Å for the Et-substituted analogue (Table 1).[36] For the five-membered-ring species **1**, the C(8)−Fe−P angle (81.98(4)°) is obviously smaller than for the acyclic analogues (Table 1), which may generate a certain degree of ring strain. However, as a result of the ring constraints, one can see that the P−Fe bond (2.1581(3) Å) becomes much smaller in comparison to those in the acyclic compounds (Table 1). This result suggests that the cyclic bidentate ligand is able to introduce a strong P−Fe bond by overcoming the phosphine steric effects. The Fe distances to other ligands are comparable for both cyclic and acyclic compounds (Table 1).

For Fp acetyl derivatives, it has been systemically studied and demonstrated that the Fe−P bond length is related to the steric effect of the alkylphosphine ligand.[41] As shown in Table 2, by

**Table 2. Comparison of Bond Angles and Distances for 2 and Its Acyclic Analogues**

| | | acyclic ($\eta^5$-$C_5H_5$)Fe(CO)(PPhRR′)C(O)R′ | |
|---|---|---|---|
| bond angle or distance | ring **2** | R = Ph; R′ = Bu[43] | R = Me; R′ = Me[41] |
| C(1)−Fe−C(6) | 92.76(7) | 92.1(4) | 94.6(2) |
| C(6)−Fe−P | 90.61(5) | 95.9(3) | 92.9(1) |
| C(1)−Fe−P | 87.89(5) | 91.3(3) | 88.2(1) |
| Fe−P | 2.169 | 2.198 | 2.180 |
| Fe−CO | 1.729 | 1.723 | 1.725 |
| Fe−C(O)R | 1.960 | 1.992 | 1.948 |

using dimethylphenylphosphine to replace the commonly used triphenylphosphine, the shortest Fe−P bond (2.180 Å) for this type of compound had been reported (Table 2).[41] However, via the formation of the cyclic Fp acyl derivative **2**, the bond can be further strengthened, leading to an even shorter P−Fe bond length of 2.169 Å. A similar bond length was also reported for a five-membered-ring Fp acetyl derivative.[42]

$^{31}P$ NMR spectra for **1** and **2** are shown in Figure S2 (Supporting Information). As shown in the figure, compounds **1** and **2** exhibit a single peak at 109 and 70 ppm, respectively. These characteristic peaks can therefore be used as indicative for the formation of the rings. $^1H$ NMR spectroscopy for **1** is illustrated in Figure 4a, in which the Cp signal appears at 4.2 ppm. This peak undergoes a 0.6 ppm upfield shift in comparison to that in FpP as a result of the coordination of phosphorus to Fe. The occurrence of the coordination created


dx.doi.org/10.1021/om4010516 | Organometallics XXXX, XXX, XXX−XXX

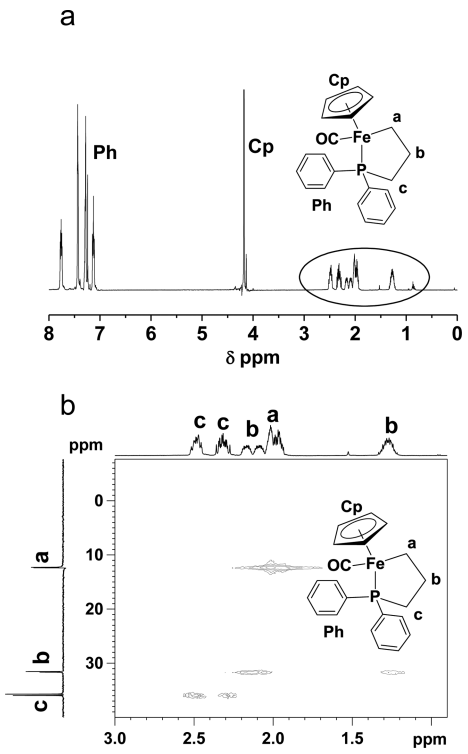


**Figure 4.** $^{1}$H NMR (a) and $^{13}$C−$^{1}$H HMBC 2D NMR (b) for **1** in $CDCl_3$.

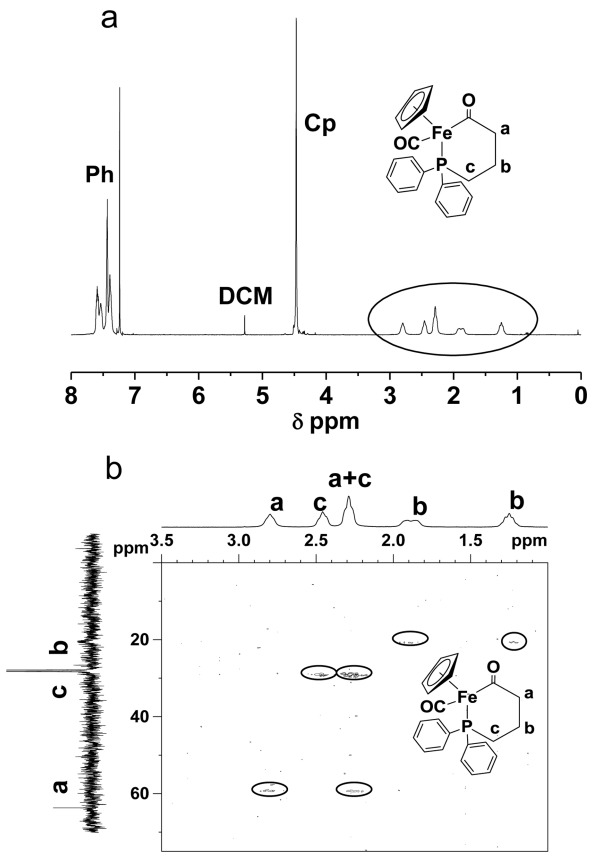


**Figure 5.** $^{1}$H NMR (a) and $^{13}$C−$^{1}$H HMBC 2D NMR (b) for **2** in $CDCl_3$.

an asymmetric Fe unit, which significantly complicated the $^{1}$H NMR spectrum of the molecule (Figure 4a). As shown in the figure, multiple chemical shifts are observed at 7.8−7.1 and 2.50−1.30 ppm, accounting for phenyl groups and the propyl spacer, respectively. To resolve the upfield peaks, $^{13}$C NMR and $^{13}$C−$^{1}$H HMQC 2D NMR were performed. In $^{13}$C NMR, the signals due to the three propyl carbons appear at 36, 31, and 12 ppm, which can be respectively assigned to the carbon adjacent to phosphorus[25] the carbons $\beta$ and $\alpha$ to Fe on the basis of the degree of the C−P coupling effect. Hydrogen to carbon connectivities are subsequently determined from the cross peaks in the 2D NMR spectrum. Consequently, chemical shifts at 2.5 and 2.3 ppm can be assigned to protons $\alpha$ to phosphorus (c in Figure 4b), the peaks at 2.0 ppm are due to the proton $\alpha$ to iron (a in Figure 4b), and $\beta$ protons appear at 2.1 and 1.3 ppm. (b in Figure 4b).

Similar to the case for **1**, compound **2** also displays multiple peaks appearing upfield due to the propyl spacer. From $^{13}$C NMR, C−P coupling with $J_{PC}$ = 32.4 Hz was only observed for the signal at 29 ppm, and no coupling effect was observed for the other two signals. Therefore, the chemical shift at 29 ppm is assigned to the carbon adjacent to phosphorus (c in Figure 5b). The carbon $\alpha$ to the acyl group appears at 68 ppm (a in Figure 5b), which is consistent with previous literature data.[25] The signal at 21 ppm is attributed to the carbon $\beta$ to the acyl group (c in Figure 5b). Subsequently, the proton peaks are assigned via the cross peaks appearing in the 2D NMR (Figure 5b).

**Effect of Concentration and Temperature on the FpP Solution Reaction.** On the basis of the above investigation, possible products produced from the FpP solution reaction can be analyzed by using $^{31}$P NMR. A representative spectrum is illustrated in Figure 6. As shown in the figure, after the solution was heated at 40 °C for 6 h, both **1** and **2** were formed, as indicated by the signals at 109 and 70 ppm, respectively. The chemical shift at −14.7 ppm is attributed to unreacted FpP. In addition, two signals at 72.8 and −13.6 ppm due to coordinated[25] and uncoordinated phosphorus are observed. The appearance of these two peaks with an intensity ratio of close to 1:1 strongly suggests the formation of FpP dimers. Taking advantage of the well-resolved chemical shifts for all products of intra- and intermolecular reactions, we further investigated solution reactions of FpP with varied concentration and temperature.

By a comparison of integration ratios, the relative conversions of FpP each species can be extracted. The resulting data for all reaction conditions are illustrated in Table 3.

It is well-known that Fp derivatives can readily release CO ligand and the reaction is light sensitive.[36] On the other hand, MIR requires a relatively higher temperature.[34] As a result, intramolecular cyclization via CO release was the major reaction when the reaction was performed at room temperature, leading to **1** in a yield of over 90% (entries 1 and 2 in Table 3). Particularly, when THF was used as solvent (entry 2 in Table 3), **1** was produced almost exclusively. When the temperature was increased to 40 and 70 °C, MIR was promoted, leading to a significant amount of products produced from either intra- or intermolecular MIR (entries 3 and 4 in Table 3). The higher the temperature, the more MIR product. When the reaction temperature was kept at 70 °C, the percentage of intermolecular products increased from 46.3 to 70.4 and 89.6% (entries 5−7 in Table 3) by carrying out the reaction with a concentration of FpP at 2%, 5% and 10%, respectively. On the basis of this investigation, migration


dx.doi.org/10.1021/om4010516 | *Organometallics* XXXX, XXX, XXX−XXX

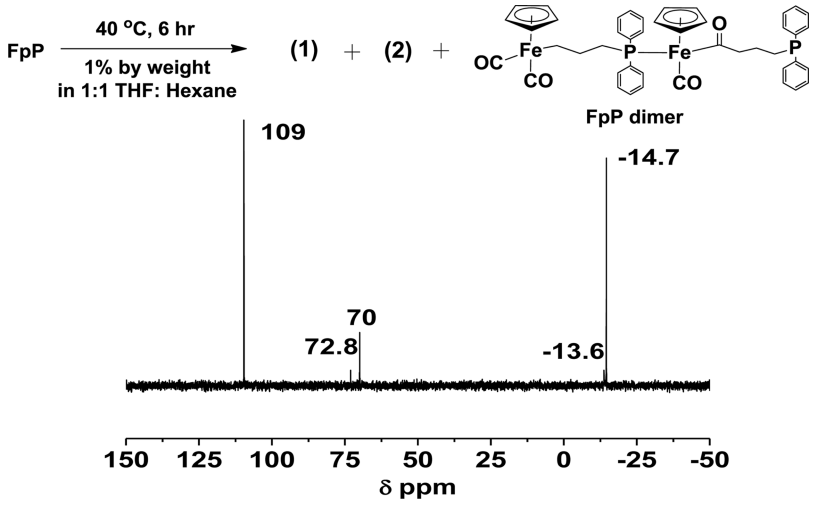


**Figure 6.** $^{31}$P NMR spectrum for the reaction solution of FpP in 1/1 THF/hexane (1% by weight, 40 °C, 6 h).

**Table 3. $^{31}$P NMR Analysis of Reaction Mixtures of FpP Solutions**

| | | | | | rel conversion (%)[a] | | |
|---|---|---|---|---|---|---|---|
| entry | solvent | temp (°C) | concentration (wt %) | time | 1 | 2 | 3 |
| 1 | hexane | 25 | 1.0 | 7 days | 93.5 | 2.8 | 3.7 |
| 2 | THF | 25 | 1.0 | 7 days | 99.8 | 0.1 | 0.08 |
| 3 | THF | 40 | 1.0 | 6 h | 76.0 | 12.8 | 11.2 |
| 4 | THF | 70 | 1.0 | 4 h | 51.8 | 36.8 | 11.40 |
| 5 | THF | 70 | 2.0 | 4 h | 13 | 40.7 | 46.3 |
| 6 | THF | 70 | 5.0 | 4 h | 8.6 | 21 | 70.4 |
| 7 | THF | 70 | 10 | 4 h | 5.0 | 5.4 | 89.6 |

[a] **1** and **2** represent intramolecular cyclic complexes, while **3** represents intermolecular MIP products, as shown in Scheme 1.

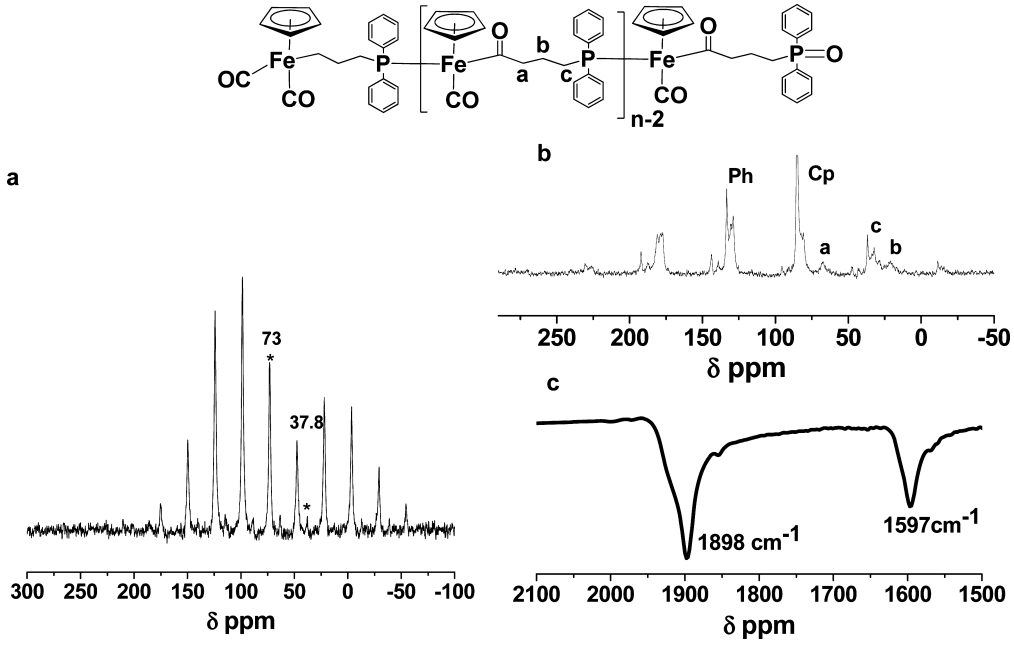


**Figure 7.** Solid-state $^{31}$P NMR (a), solid-state $^{13}$C NMR (b), and FT-IR (c) for the insoluble materials produced from solution MIP of FpP.

insertion polymerization of FpP is possible if an FpP solution with a high concentration is heated at an elevated temperature.

**Solution Polymerization.** Solution polymerization of FpP in THF with concentration of ca. 20% by weight was performed at 70 °C. After the solution was heated for 1 h, it was noticed that there was insoluble material produced and suspended in the solution. The insoluble fraction was separated from the THF solution via centrifugation at the end of the polymerization. The clear supernatant was then added dropwise into hexane, yielding pale yellow precipitates. The weight ratio of these two fractions (insoluble to soluble products) is ca. 30:70. The THF-insoluble fraction also appears to be the same color


dx.doi.org/10.1021/om4010516 | Organometallics XXXX, XXX, XXX−XXX

and looks similar to the THF-soluble products. The insoluble polymers were characterized by using solid-state $^{31}$P NMR and $^{13}$C NMR. As shown in Figure 7a, $^{31}$P NMR reveals two peaks at 73 and 37.8 ppm along with multiple spinning sidebands. These two peaks can be assigned to the main-chain coordinated phosphorus and the oxidized phosphine end group. The solid-state $^{13}$C NMR spectrum is illustrated in Figure 7b. As shown in the figure, the signals for the phenyl group appear at 125−130 ppm; the peaks between 85 and 88 ppm are assigned to the Cp ring. The resonance signal at 67 ppm is due to the carbon next to the acyl group. The two peaks at 32 and 36 ppm, due to C−P coupling, arise from the carbon adjacent to the phosphorus. The carbon in the middle of the spacer appears at 20 ppm. All of these assignments are similar to the corresponding signals in the solution $^{13}$C NMR of THF-soluble PFpP. However, the chemical shift for the carbonyl groups is invisible due to weak $^{1}$H−$^{13}$C cross-polarization for carbonyl carbon. FT-IR was then used for the characterization. As shown in Figure 7c, two peaks at 1898 and 1597 cm$^{-1}$ are observed, which correspond to the terminal carbonyl and migrated carbonyl groups, respectively.[31] The existence of these two types of carbonyl groups suggests that the insoluble materials are the products resulting from migratory insertion reactions. The reason for the formation of insoluble PFpP is a matter for further research.

The molecular weight of the THF-soluble fraction was determined by GPC. As illustrated in Figure 8a, the GPC curve

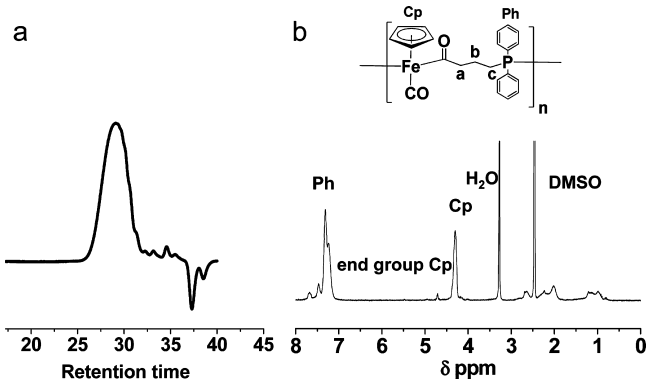


**Figure 8.** GPC curve for PFpP (a) and $^{1}$H NMR of PFpP in DMSO-$d_6$ produced via solution polymerization of FpP in THF (b).

exhibits a molecular weight of 4200 g/mol with a PDI value of 1.24. The polymer structure was characterized using $^{1}$H NMR (Figure 8b). In $^{1}$H NMR, the chemical shifts at 7.8−7.1 and 4.3 ppm represent the phenyl groups and Cp rings in each Fp acyl repeat unit. The integration ratio of these two peaks is 1:2, which is in agreement with the expected structure. The signal at 4.8 ppm represents the Cp ring for the Fp end group of the polymer. Intensities of the chemical shifts for Cp at 4.3 and 4.8 ppm are compared for end group analysis, suggesting that the polymer has a DP value of 11. The molecular weight estimated from the analysis is ca. 4400, which is in agreement with the GPC results. Chemical shifts for the propyl spacer appeared between 0.8 and 2.7 ppm.

$^{13}$C−$^{1}$H HMQC 2D NMR was performed to assign the signal for the propyl spacer. The correlation map shows that the signals at 2.8 and 2.3 ppm in $^{1}$H NMR connect to the same peak at 66 ppm due to the acyl group in $^{13}$C NMR (a in Figure 9), suggesting that the two protons from C(O)CH$_2$ are

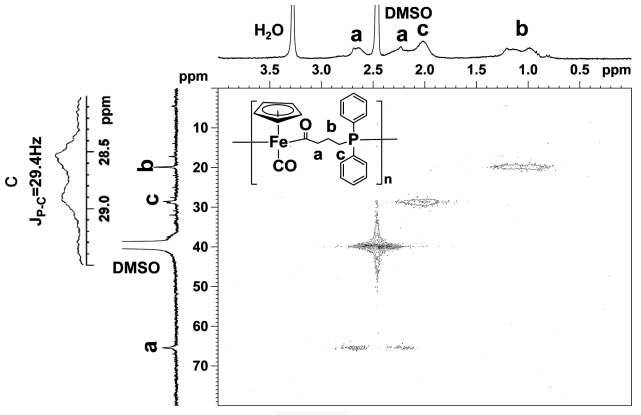


**Figure 9.** $^{13}$C−$^{1}$H HMQC 2D NMR for PFpP.

diastereotopic. Expanded $^{13}$C NMR indicates that there are double peaks at 29 ppm due to C−P coupling (c in Figure 9), suggesting that this carbon is adjacent to the phosphorus. In contrast, the peak at 20 ppm (b in Figure 9) is a singlet, indicating a weak C−P coupling effect. Therefore, the peak at 20 ppm can be assigned to the carbon $\beta$ to the iron center. From the cross peaks observed in Figure 9, the signal at 1.9−2.2 ppm in $^{1}$H NMR can be assigned to the proton on the carbon adjacent to PPh$_2$, while the peak at 0.9−1.3 ppm is due to the protons $\beta$ to the iron center.

During the polymerization, samples were withdrawn at certain intervals and used for $^{31}$P NMR analysis. $^{31}$P NMR spectra are compared in Figure 10. Signal at −14.7 ppm is due to the monomers ($P_0$ in Figure 10a).[31] The chain end coordinated phosphorus for dimers and other species with DP more than 2 can be distinguished in the $^{31}$P NMR. As illustrated in the Figure, signal at 72.8 ppm can be assigned to dimers ($P_1$ in Figure 10a) and that at 72.6 ppm is due to PFpP with DP larger than 2 ($P_2$ in Figure 10a). As shown in the Figure, with the progress of the polymerization, the peak at −14.7 ppm gradually decreased, which is accompanied by increased intensities for the peaks due to coordinated backbone phosphorus suggesting polymerization occurred (Figure S3). As shown in Figure 10b, dimers were preferentially formed as indicated by the appearance of the signal at 72.8 ppm when the solution was heated for 30 min. These dimers converted to longer chains over time as indicated by increased intensities for the peaks at 72.6 ppm (Figure 10b) and the peaks around 74 ppm due to the backbone phosphorus (Figure S3). As expected, the monomer consumption is much faster than the step-growth of the dimers. After polymerization for 5 h, although over 90% of FpP was consumed, 50% of the coordinated products are dimers as estimated from the integration ratio between the signals at 72.8 and 72.6 ppm. Small amount of dimers (16.6%) still remained in the solution even all monomers were consumed after 19 h (Figure 10b). The NMR analysis indicates that the polymerization follows a typical step-growth mechanism.

## CONCLUSION

Cyclcopentadienyldicarbonyl[(diphenylphosphino)propyl]iron (FpP) was synthesized and fully characterized. In solution, FpP undergoes both intra- and intermolecular reactions depending on the conditions. Reactions with lower FpP concentration (ca. 1% by weight) at 25 °C favor the formation of five-membered rings via CO release, while at a higher temperature (70 °C),


dx.doi.org/10.1021/om4010516 | Organometallics XXXX, XXX, XXX−XXX

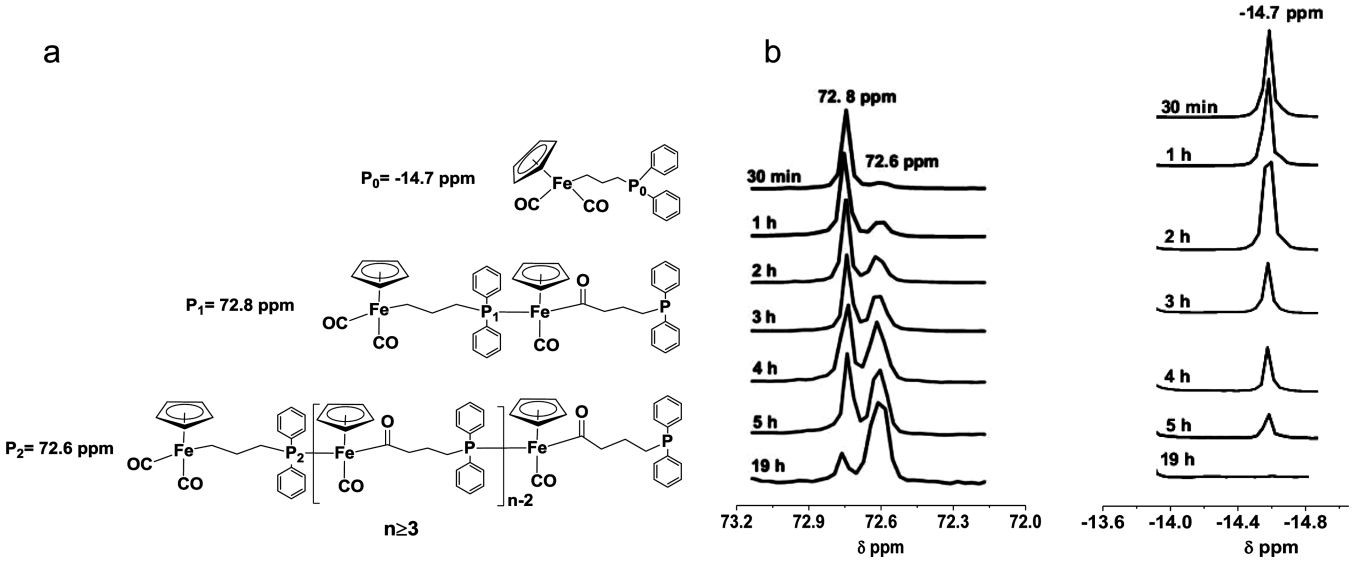


**Figure 10.** Chemical structures for FpP, FpP dimer and PFpP with DP larger than 2 ($P_0$, $P_1$, $P_2$ respectively correspond to phosphorus in FpP, coordinated phosphorus in FpP dimer and terminal repeat unit of PFpP with DP larger than 2) (a); Intensities for chemical shifts in the $^{31}P$ NMR at −14.7 ppm ($P_0$), 72.6 ppm ($P_1$) and 72.8 ppm ($P_2$) as a function of polymerization time (b).

MIR was promoted, generating six-membered rings as major products when the FpP concentration was low. Intermolecular MIR was promoted by increasing the FpP concentration. Polymerization of FpP in a highly concentrated solution (20% by weight) was therefore performed at 70 °C, leading to both THF-soluble and -insoluble polymers. Both soluble and insoluble polymers appear similar in color. The soluble polymers have $M_n$ values of ca. 4200 with a PDI value of 1.24 as characterized by GPC. FT-TR and solid-state NMR analysis of the insoluble products indicates that they were also generated via migration insertion polymerization. These comprehensive studies of FpP chemical reactions in solution offer valuable fundamental knowledge required for further exploration of the newly developed MIP.

## EXPERIMENTAL SECTION

**Materials and Instrumentation.** All experiments were performed under an atmosphere of dry nitrogen using either standard Schlenk techniques or a glovebox unless otherwise indicated. THF was freshly distilled under nitrogen from Na/benzophenone. Hexane was degassed with dry nitrogen. Toluene was dried with molecular sieves before use. Sodium (Na), 1-bromo-3-chloropropane, and potassium (K) were purchased from Sigma-Aldrich. Cyclopentadienyliron dicarbonyl dimer ($Fp_2$) was purchased from Strem Chemicals Inc. Chlorodiphenylphosphine was purchased from Tokyo Chemical Industry (TCI). Benzophenone was purchased from Fisher Scientific. All chemicals were used as received unless otherwise indicated.

$^1H$, $^{31}P$, and $^{13}C$ NMR and heteronuclear multiple quantum coherence (HMQC) and correlation spectroscopy (COSY) spectra were obtained on a Bruker Avance 300 ($^1H$, 300 MHz; $^{31}P$, 120 MHz; $^{13}C$, 75 MHz) spectrometer at ambient temperature using the appropriate solvents. NMR samples were prepared under an atmosphere of dry nitrogen unless otherwise indicated.

Solid-state $^{13}C$ NMR was performed on a Bruker Avance 500 ($^{13}C$, 125 MHz) spectrometer at ambient temperature with cross-polarization and magic angle spinning. The contact time and spinning rate were 2 ms and 6.1 kHz, respectively. The pulse program cpramp was used. A total of 2 K scans was collected. The low-frequency $^{13}C$ signal at 29.5 ppm from admantane was used as an external reference to determine the chemical shifts.

Solid-state $^{31}P$ NMR spectra were recorded on a Bruker Avance 500 ($^{31}P$, 202 MHz) spectrometer at ambient temperature. High-power decoupling with magic angle spinning was employed. The relaxation time and spinning rate were 20 s and 5.2 kHz, respectively. The hpdec program was used. A total of 2 K scans was accumulated. Chemical shifts were determined with respect to the external signal for ammonium dihydrogen phosphate at 0.81 ppm.

Fourier transform infrared spectroscopy (FT-IR) was carried out as Nujol mulls between KBr plates using a Perkin-Elmer Spectrum RX I FT-IR system.

Molecular weights and molecular distributions, $M_w/M_n$, were characterized by GPC at room temperature with THF as eluent at a flow rate of 1.0 mL/min on a system consisting of a Waters 510 HPLC pump, Jordi DVB mixed-bed linear columns (500 mm × 10 mm, molecular weight range $10^2$–$10^7$), and a Waters 410 differential refractometer detector. Calibration parameters were obtained using standard polystyrene samples.

Single crystals suitable for X-ray diffraction analysis were mounted onto the tips of glass fibers with a thick oil and transferred immediately into the cold nitrogen gas stream of the diffractometer cryostat. X-ray data were collected using Mo $K\alpha$ radiation at 200 K on a Bruker Kappa APEX II System (Madison, WI, USA). Structures were solved using direct methods and refined by full-matrix least squares on $F_2$ using the APEX2 package (v2012.4.0).

**Synthesis of Sodium Diphenylphosphide ($Ph_2PNa$).** $Ph_2PNa$ was prepared by heating sodium and $ClPPh_2$ at 40 °C for 3 days. The resulting orange solution was directly used for further reactions. $^{31}P$ NMR (THF): −23 ppm.

**Synthesis of 3-Chloropropyldiphenylphosphine.** A 250 mL Schlenk flask was charged with a solution of $BrCH_2CH_2CH_2Cl$ (7.87 g, $5.0 \times 10^{-2}$ mol) in dry THF (50 mL). To this solution was added $Ph_2PNa$ (0.5 M in THF solution; 60 mL, $3.0 \times 10^{-2}$ mol) dropwise at 0 °C. The mixture was then warmed to room temperature and stirred overnight. After the reaction, the solvent and excess $BrCH_2CH_2CH_2Cl$ were removed at 60 °C for ca. 2 h under vacuum. The residue was dissolved in a minimum amount of hexane and the solution filtered through a silica gel column. Hexane was then removed under vacuum at room temperature, yielding a colorless oil (5.52 g, 70% yield). $^1H$ NMR ($CDCl_3$): 7.45 and 7.35 (d, 10 H, aromatic protons), 3.60 (t, 2H, $CH_2Cl$), 2.20 (t, 2H, $CH_2P$), 1.92 ppm (m, $CH_2CH_2CH_2$). $^{31}P$ NMR: −14.7 ppm.

**Synthesis of FpP..**[44,45] A solution of $Ph_2PCH_2CH_2CH_2Cl$ (1.01 g, $3.8 \times 10^{-3}$ mol) in THF (5 mL) was added dropwise to an orange suspension of FpK[46] (1.00 g, $4.6 \times 10^{-3}$ mol) in THF (25 mL) at 0 °C. The reaction flask was wrapped with aluminum foil in order to exclude light. The mixture was stirred at room temperature for 2 h.


dx.doi.org/10.1021/om4010516 | Organometallics XXXX, XXX, XXX−XXX

The THF was then removed under vacuum, and degassed hexane was added to dissolve the crude product. The hexane solution was transferred using a cannula into another Schlenk flask. After removing solvent, an oil-like crude product was obtained. The oil was then dissolved in a minimum amount of hexane/DCM (4/1, v/v) and the solution filtered on a short silica gel column to remove dimers which were formed during the reaction. The bright yellow solution was collected, and solvents were subsequently removed under vacuum, generating a bright yellow powder. The yellow powder was crystallized from hexane at −49 °C to yield yellow crystals. Yield: 1.1 g (60%) $^1$H NMR (DMSO-$d_6$): 7.35 (t, 4 H, ortho $C_6H_5$), 7.32 (m, 6 H, para, meta $C_6H_5$), 4.87 (s, 5H, $C_5H_5$), 2.07 (2H, $PCH_2$), 1.46 ppm (4H, $FeCH_2CH_2$). $^1$H NMR ($C_6D_6$): 7.61 (t, 4 H, ortho $C_6H_5$), 7.20 (m, 6 H, para, meta $C_6H_5$), 4.03 (s, 5H, $C_5H_5$),[47] 2.25 (t, 2H, $PCH_2$), 1.80 (m, 2H, $CH_2CH_2CH_2$), 1.64 ppm (t, 2H, $Fe-CH_2$). $^{31}$P NMR (DMSO-$d_6$): −14.7 ppm. $^{31}$P NMR ($C_6D_6$): −14.4 ppm. $^{13}$C NMR (DMSO-$d_6$): 5 ($FpCH_2$, $^3J_{PC}$ = 11.4 Hz), 32.5 ($CH_2CH_2P(Ph)_2$, $^2J_{PC}$ = 15.3 Hz), 34.3 ($CH_2P(Ph)_2$, $^1J_{PC}$ = 14 Hz), 87 ($C_5H_4$), 129, 132, 139 (*Ph*), 218 ppm ($FeC{\equiv}O$).[44] FT-IR (Nujol mull): 2004 and 1952 cm$^{-1}$ (terminal CO stretching).

**Synthesis of Cyclopentadienyl(carbonyl)[3-(diphenylphosphanyl-κ*P*)prop-1-yl]iron (1) from FpP.** FpP was dissolved in THF (concentration 10 mg/mL) and stirred at room temperature for 7 days at room temperature. THF was subsequently removed under vacuum, yielding an orange oil. The orange oil was chromatographed on a silica gel column with hexane/ethyl acetate (10/1 v/v) as eluent. The yellow band was collected, and the solvent was removed under high vacuum, yielding an orange oil. The resulting oil was recrystallized from a minimum amount of hexane at −49 °C. Yield: 70%. $^1$H NMR ($CDCl_3$): 7.76, 7.49, 7.33, and 7.15 (10H, $C_6H_5$), 4.21 (s, 5H, $C_5H_5$), 2.50 (m, $^1$H, $PCH_2$), 2.30 (m, $^1$H, $PCH_2$), 2.10 , (m, $^1$H, $CH_2CH_2CH_2$), 1.30 (m, $^1$H, $CH_2CH_2CH_2$), 2.0 ppm (m, 2H, $FeCH_2$). $^{13}$C NMR ($CDCl_3$): 36 (d, $PCH_2$, $^1J_{PC}$ = 31.2 Hz), 31 (d, $CH_2CH_2CH_2$, $^2J_{PC}$ = 12.8 Hz), 12 (d, $FeCH_2$, $^3J_{PC}$ = 10.9 Hz). 82.6 ppm (s, $C_5H_5$), 134, 130, and 128 ppm ($C_6H_5$). $^{31}$P NMR ($CDCl_3$): 109 ppm.

**Synthesis of Cyclopentadienyl(carbonyl)[(4-diphenylphosphanyl-κ*P*)butanoyl]iron (2) from FpP.** FpP was dissolved in THF (concentration 10 mg/mL), and the reaction mixture was heated at 70 °C for 2 h in the dark (covered by aluminum foil). After the mixture was cooled to room temperature, the solvent was removed under vacuum, yielding a yellow oil. The yellow oil was further purified using chromatography on a silica gel column. Hexane/EA (2.5/1 v/v) was used as eluent. The resulting oil was recrystallized from DCM/hexane (1/5 v/v) at −49 °C, yielding yellow crystals. Yield: 55%. $^1$H NMR ($CDCl_3$): 7.62, 7.48 (10H, $C_6H_5$), 4.52 (*s*, 5H, $C_5H_5$), 2.84 (t, 1H, $COCH_2$), 2.33 (m, 1H, $COCH_2$), 2.50 (*m*, 1H, $PCH_2$), 2.33 (m, 1H, $PCH_2$), 1.91 (m, 1H, $CH_2CH_2CH_2$), 1.30 ppm (m, 1H, $CH_2CH_2CH_2$). $^{13}$C NMR (Dept-135, $CDCl_3$): 68 (s, $COCH_2$), 29 (d, $PCH_2$, $^1J_{PC}$ = 32.4 Hz), 21 (*b*, $CH_2CH_2CH_2$). 82.6 (*s*, $C_5H_5$), 134, 130, and 128 ppm ($C_6H_5$). $^{31}$P NMR ($CDCl_3$): 70 ppm.

**Solution Polymerization of FpP.** FpP was dissolved in THF (20% by weight) and heated to 70 °C. At certain time intervals, samples were withdrawn for $^{31}$P NMR analysis. After 19 h, the solution was cooled to room temperature and centrifuged to separate the suspended solids. The clear yellow supernatant was added dropwise to hexane to precipitate PFpP. Both the THF-insoluble product and the precipitate were collected and dried under vacuum at room temperature overnight. The resulting polymers (THF-insoluble and -soluble fractions) are bright yellow powders. The weight ratio for the two fractions is ca. 30:70. THF-insoluble fraction: solid state $^{13}$C NMR 20 ($CH_2CH_2CH_2$) 32, 36 ($PCH_2$), 67 ($CH_2C{=}O$), 85−88 ($C_5H_5$), 125−130 ppm ($C_6H_5$); solid-state $^{31}$P NMR 73 and 37.8 ppm; FT-IR 1898 (terminal CO stretch), 1597 cm$^{-1}$ (ketonic CO stretch). THF-soluble fraction: $^1$H NMR (DMSO-$d_6$) 7.8−7.1 (b, 10H, $C_6H_5$), 4.4−4.2 (b, 5H, $C_5H_5$), 2.78−2.60 (b, 1H, $COCH_2$), 2.47−2.17 (b, 1H, $COCH_2$), 2.13−1.89 (b, 2H, $CH_2P$), and 1.32−0.74 ppm (b, 2H, $CH_2CH_2CH_2$); $^{13}$C NMR (DMSO-$d_6$) 20 (s, $CH_2CH_2CH_2$), 29 (d, $PCH_2$, $^1J_{PC}$ = 29.4 Hz), 66 (s, $CH_2C{=}O$), 84, 86 ($C_5H_5$), 127, 128, 129, 130, 132 ($C_6H_5$), 220, 217 (d, s, $C{\equiv}O$), and 274 ppm (s, $CH_2C{=}O$); $^{31}$P NMR ($CDCl_3$) 73.4, 72.3, and −13.6 ppm; FT-IR 1910 (terminal CO stretch), 1600 cm$^{-1}$ (ketonic CO stretch).

## ■ ASSOCIATED CONTENT

### Ⓢ Supporting Information

Tables, figures, and CIF files giving crystal data for compounds FpP, **1**, and **2** (CCDC nos. 963926−963928) and $^{13}$C NMR $^{13}$C− $^1$H HMQC 2D NMR, and $^{31}$P NMR. This material is available free of charge via the Internet at http://pubs.acs.org.

## ■ AUTHOR INFORMATION


### Corresponding Author

*E-mail: bill.power@uwaterloo.ca (W.P.P.); xiaosong.wang@uwaterloo.ca (X.W.).


### Notes

The authors declare no competing financial interest.

## ■ ACKNOWLEDGMENTS


X.W. is grateful for the financial support of the NSERC of Canada and the University of Waterloo.


## ■ REFERENCES


(1) Manners, I. *Synthetic Metal Containing Polymers*; Wiley-VCH: Weinheim, Germany, 2004.
(2) Whittell, G. R.; Hager, M. D.; Schubert, U. S.; Manners, I. *Nat. Mater.* **2011**, *10*, 176.
(3) Wang, X.; McHale, R. *Macromol. Rapid Commun.* **2010**, *31*, 331.
(4) Ramanathan, M.; Tseng, Y. C.; Ariga, K.; Darling, S. B. *J. Mater. Chem. C* **2013**, *1*, 2080.
(5) Abd-El-Aziz, A. S.; Strohm, E. A. *Polymer* **2012**, *53*, 4879.
(6) Wong, W.-Y.; Wang, X.-Z.; He, Z.; Djurisic, A. B.; Yip, C.-T.; Cheung, K.-Y.; Wang, H.; Mak, C. S. K.; Chan, W.-K. *Nat. Mater.* **2007**, *6*, 521.
(7) Arsenault, A. C.; Miguez, H.; Kitaev, V.; Ozin, G. A.; Manners, I. *Adv. Mater.* **2003**, *15*, 503.
(8) Dong, Q.; Li, G.; Ho, C.-L.; Faisal, M.; Leung, C.-W.; Pong, P. W.-T.; Liu, K.; Tang, B.-Z.; Manners, I.; Wong, W.-Y. *Adv. Mater.* **2012**, *24*, 1034.
(9) Zha, Y.; Disabb-Miller, M. L.; Johnson, Z. D.; Hickner, M. A.; Tew, G. N. *J. Am. Chem. Soc.* **2012**, *134*, 4493.
(10) Zha, Y.; Thaker, H. D.; Maddikeri, R. R.; Gido, S. P.; Tuominen, M. T.; Tew, G. N. *J. Am. Chem. Soc.* **2012**, *134*, 14534.
(11) Kishimura, A.; Yamashita, T.; Yamaguchi, K.; Aida, T. *Nat. Mater.* **2005**, *4*, 546.
(12) He, F.; Gadt, T.; Manners, I.; Winnik, M. A. *J. Am. Chem. Soc.* **2011**, *133*, 9095.
(13) Ma, Y.; Dong, W.-F.; Hempenius, M. A.; Mohwald, H.; Vancso, G. J. *Nat. Mater.* **2006**, *5*, 724.
(14) Hasegawa, U.; van der Vlies, A. J.; Simeoni, E.; Wandrey, C.; Hubbell, J. A. *J. Am. Chem. Soc.* **2010**, *132*, 18273.
(15) Burnworth, M.; Tang, L.; Kumpfer, J. R.; Duncan, A. J.; Beyer, F. L.; Fiore, G. L.; Rowan, S. J.; Weder, C. *Nature* **2011**, *472*, 334.
(16) Wang, X.; Guerin, G.; Wang, H.; Wang, Y.; Manners, I.; Winnik, M. A. *Science* **2007**, *317*, 644.
(17) Mapolie, S. F.; Moss, J. R.; Smith, G. S. *Appl. Organomet. Chem.* **1998**, *12*, 801.
(18) Sharma, H. K.; Cervantes-Lee, F.; Pannell, K. H. *J. Am. Chem. Soc.* **2004**, *126*, 1326.
(19) Zhang, J.; Ren, L.; Hardy, C. G.; Tang, C. *Macromolecules* **2012**, *45*, 6857.
(20) Chadha, P.; Ragogna, P. J. *Chem. Commun.* **2011**, *47*, 5301.
(21) Tonhauser, C.; Alkan, A.; Schomer, M.; Dingels, C.; Ritz, S.; Mailander, V.; Frey, H.; Wurm, F. R. *Macromolecules* **2013**, *46*, 647.
(22) Jennings, D. M.; Brady, S. E.; Shultz, G. V.; Zakharov, L. N.; Tyler, D. R. *Polym. Bull.* **2012**, *68*, 2243.

(23) Miles, D.; Burrow, T.; Lough, A.; Foucher, D. *J. Inorg. Organomet. Polym. Mater.* **2010**, *20*, 544.
(24) Gladysz, J. A. *Organometallics* **2011**, *30*, 1.
(25) Kumar, M.; Metta-Magana, A. J.; Sharma, H. K.; Pannell, K. H. *Dalton Trans.* **2010**, *39*, 7125.
(26) Shusterman, A. J.; Tamir, I.; Pross, A. *J. Organomet. Chem.* **1988**, *340*, 203.
(27) Berke, H.; Hoffmann, R. *J. Am. Chem. Soc.* **1978**, *100*, 7224.
(28) Nomura, K.; Zhang, S. *Chem. Rev.* **2011**, *111*, 2342.
(29) Drent, E.; Budzelaar, P. H. M. *Chem. Rev.* **1996**, *96*, 663.
(30) Wu, G.-P.; Ren, W.-M.; Luo, Y.; Li, B.; Zhang, W.-Z.; Lu, X.-B. *J. Am. Chem. Soc.* **2012**, *134*, 5682.
(31) Wang, X. S.; Cao, K.; Liu, Y. B.; Tsang, B.; Liew, S. *J. Am. Chem. Soc.* **2013**, *135*, 3399.
(32) McWilliams, A.; Dorn, H.; Manners, I. In *New Aspects in Phosphorus Chemistry I*; Majoral, J.-P., Ed.; Springer: Berlin/Heidelberg, Germany, 2002; Vol. *220*, p 141.
(33) Noonan, K. J. T.; Gillon, B. H.; Cappello, V.; Gates, D. P. *J. Am. Chem. Soc.* **2008**, *130*, 12876.
(34) Green, M.; Westlake, D. J. *J. Chem. Soc. A* **1971**, 367.
(35) Bibler, J. P.; Wojcicki, A. *Inorg. Chem.* **1966**, *5*, 889.
(36) Davies, S. G.; Dordorhedgecock, I. M.; Sutton, K. H.; Whittaker, M. *J. Am. Chem. Soc.* **1987**, *109*, 5711.
(37) Pope, L.; Sommerville, P.; Laing, M.; Hindson, K. J.; Moss, J. R. *J. Organomet. Chem.* **1976**, *112*, 309.
(38) Quin, L. D. *A Guide to Organophosphorus Chemistry*; Wiley: Hoboken, NJ, 2000.
(39) Wedge, T. J.; Herzog, A.; Huertas, R.; Lee, M. W.; Knobler, C. B.; Hawthorne, M. F. *Organometallics* **2004**, *23*, 482.
(40) Davies, S. G.; Dordorhedgecock, I. M.; Sutton, K. H.; Whittaker, M. *J. Organomet. Chem.* **1987**, *320*, C19.
(41) Liu, H. Y.; Eriks, K.; Giering, W. P.; Prock, A. *Acta Crystallogr., Sect. C: Cryst. Struct. Commun.* **1992**, *48*, 433.
(42) Ashby, M. T.; Enemark, J. H. *Organometallics* **1987**, *6*, 1318.
(43) Liu, L. K.; Luh, L. S. *Organometallics* **1994**, *13*, 2816.
(44) Emeran, A.; Gafoor, M. A.; Goslett, J. K. I.; Liao, Y. H.; Pimble, L.; Moss, J. R. *J. Organomet. Chem.* **1991**, *405*, 237.
(45) Moss, J. R. *J. Organomet. Chem.* **1982**, *231*, 229.
(46) Plotkin, J. S.; Shore, S. G. *Inorg. Chem.* **1981**, *20*, 284.
(47) Scharrer, E.; Brookhart, M. *J. Organomet. Chem.* **1995**, *497*, 61.